RSC Advances

PAPER

View Article Online
View Journal | View Issue

Cite this: *RSC Adv.*, 2017, **7**, 13097

Controlling the conductivity of Ti_3C_2 MXenes by inductively coupled oxygen and hydrogen plasma treatment and humidity

Florian M. Römer,*[a] Ulf Wiedwald,[a] Tanja Strusch,[a] Joseph Halim,[b] Elisa Mayerberger,[b] Michel W. Barsoum[b] and Michael Farle[a]

Received 29th November 2016
Accepted 14th February 2017

DOI: 10.1039/c6ra27505b

rsc.li/rsc-advances

We report on the effects of plasma treatment and humidity on the electrical conductivities of Ti_3C_2 MXene thin films. The latter – spincoated from a colloidal solution produced by LiF/HCl etching of Ti_3AlC_2 powders – were 13 nm thick with an area of 6.8 mm^2. The changes in the films exposed to hydrogen (H) and oxygen (O) plasmas in vacuum were analyzed by X-ray photoelectron spectroscopy. We find that the film resistivities can be switched reproducibly by plasma treatment between 5.6 μΩm (oxidized state) to 4.6 μΩm (reduced state). Both states show metallic like conductivity. In high vacuum, the film resistivity was 243 Ω; when the relative humidity was 80% the film resistance increased to 6340 Ω, a 26 fold increase.

1 Introduction

Two dimensional (2D) materials have garnered huge interest in the scientific community due to their extraordinary electronic, chemical, optical, mechanical and structural properties.[1] This interest started with the isolation of a single layer of carbon (graphene) and the determination of its electronic characteristics.[2] Since then 2D materials have been of interest as sensing materials for various types of sensors.[3,4] For instance, graphene demonstrated a potential as a sensing material for electrochemical sensors,[5] hydrogen peroxide,[6] glucose,[7] nucleic acids,[7] and protein markers detectors[8] for biological sensors. In addition gases such as nitrogen oxide, NO_2,[9] hydrogen sulphide H_2S,[10] H_2 [11] and ammonia, NH_3,[12] can be detected. Similarly, other 2D materials such as transition metal dichalcogenides have demonstrated potential as materials for gas sensing and optoelectronic devices.[13,14] For example, Li *et al.* fabricated transistors made from single- and few-layers MoS_2 sheets that act as sensitive detectors for nitrous oxide NO gas.[15] He *et al.* fabricated a flexible MoS_2 thin film that demonstrated sensitivity of detection also for NO_2 gas.[16] Furthermore, the resistances of thin VS_2 films were shown to demonstrate sensitivity to moisture.[17] The main principle of 2D sensor devices is based upon changes in their conductance due to the adsorption of chemical or biological species which can act as electron donors or acceptors.[18]

Recently a new family of 2D transition metal carbides labelled MXene was discovered.[19] MXenes are produced by the selective etching of the A layers from the MAX phases.[20] The latter, in turn, are a large family of layered ternary transition metal carbides, with a chemical formula $M_{n+1}AX_n$ where M is an early transition metal, A is an A-group element (mostly groups 13 and 14) of the periodic table of elements, X is C or/and N and $n = 1$ to 3. Because during etching the A-group element, typically Al, is replaced by –O, –OH and –F terminations,[21,22,23] the proper designation of the resulting 2D material is $M_{n+1}C_nT_x$, where T represents a surface termination. MXenes have been fabricated in the form of multilayers[19] and films.[24] Thin films of $Ti_3C_2T_x$ were fabricated *via* various methods such as magnetron sputtering of the MAX phase on a sapphire substrate followed by etching of Al using HF or NH_4HF_2,[24,26] or through directly coating substrates with a colloidal solution of MXene by spray coating,[25] spin coating[26] or electrohydrodynamic atomization.[27] The most studied MXene to date is $Ti_3C_2T_x$ which has already shown potential for use in a number of diverse applications, such as batteries,[28,29,30] supercapacitors,[31,32] fuel cells,[33] transparent conducting electrodes,[24] photocatalytic applications,[34] and water treatment.[35] Most of the studies investigated thin films, but single flakes were also characterized by Miranda *et al.*[36].

Furthermore, MXenes demonstrated potential as sensors. Nanocomposites of TiO_2–$Ti_3C_2T_x$ displayed good performance and excellent long term stability for sensing H_2O_2, making it promising for biosensors applications.[37,38] Multilayered $Ti_3C_2T_x$ was used to immobilize hemoglobin to fabricate a mediator-free biosensor showing good protein bioactivity and stability.[18,37] Xu *et al.* demonstrated the capability of using a few layers of $Ti_3C_2T_x$ in a field effect transistor (FET) for probing neural activity and detecting neural transmitters.[39] Moreover, several

[a]*Faculty of Physics and Center for Nanointegration (CENIDE), University of Duisburg-Essen, Lotharstr. 1, 47057 Duisburg, Germany. E-mail: florian.roemer@uni-due.de; Tel: +49 203 379 4411*

[b]*Department of Materials Engineering, LeBow Engineering Center 27-445, Drexel University, Philadelphia, PA 19104-2875, USA*

theoretical studies showed the potential of MXenes to be used as gas sensing materials.[40,41]

Of special interest herein is the work of Dillon *et al.*[26] who characterized spin coated $Ti_3C_2T_x$ films. They showed that the conductivities of these films are a function of atmosphere; when stored in dry N_2 the sheet conductance was greater than when the films were stored in the open atmosphere or humid N_2. They also showed that the figures of merits of these transparent conductive films rivalled those of chemical vapor deposited undoped graphene films.

The purpose of this work is twofold. The first is to shed some more light on the effect of humidity on transport properties and its possible application as nanosize sensors. The second is to explore methods to further enhance their conductivities in general. To that effect we measured the conductivities of spin coated films after exposure to oxygen and hydrogen plasmas. We also measured the transport properties as a function of humidity and compared the response to a commercial humidity sensor.

2 Experimental details

2.1 Sample preparation

2.1.1 Ti_3AlC_2 synthesis. Solid Ti_3AlC_2 was produced *via* mixing Ti_2AlC powders (−325 mesh†) and TiC‡ and heating to 1350 °C (1623 K) using a heating rate of 10 K min^{-1} followed by a 2 h soak, as previously reported.[21] The resulting brick was milled and sieved (−400 mesh → mesh hole diameter 38 μm) to produce powders under 38 μm in size.

2.1.2 Delaminated Ti_3C_2 synthesis. The Ti_3AlC_2 powder was slowly added to a 12 mol/1 HCl and 7.5 molar equivalent LiF solution in a ratio of 1 g Ti_3AlC_2 : 10 ml etching solution for 24 h at 35 °C. The powders were washed *via* a centrifugation and decantation process with three washes each of 6 mol/1 HCl§, 1 mol/1 LiCl, and distilled water in the ratio of 40 ml of solvent to 0.5 g of MAX powder. Approximately 10 ml of distilled water was added to the reaction mixture after the final decantation, shaken using a mechanical agitator to disperse the sediment throughout the solution, and sonicated for 1 h at room temperature under argon (Ar) gas. The mixture was centrifuged at 5000 rpm for 1 h followed by sonication, and the supernatant was collected.

This procedure results in an optimized delamination and cleanliness: a mixture of HCl and LiF is used to convert MAX phase Ti_3AlC_2 to $Ti_3C_2T_x$ where the Al layers are selectively etched and replaced by a mixture of surface terminations:[23] O, OH and/or F in addition to the intercalation of Li ions. However LiF can not be washed sufficiently using just water, so several washes with HCl were required to remove all the LiF residual salts but this also removes the Li ions between the layers. The latter is necessary for delamination. In order to intercalate Li ions back to the MXene, washing MXene in LiCl is required. LiCl is soluble in water and can be easily washed with it while preserving the Li ions intercalated in MXene.[42]

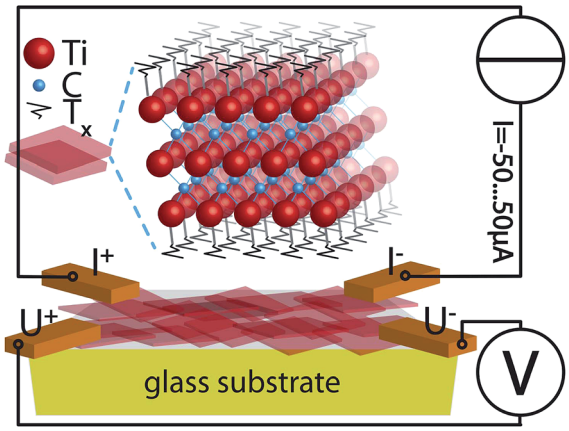

Fig. 1 Schematics of the resistivity measurement. Sheets (semi transparent red) of Ti_3C_2 are stacked on a glass substrate. The stacked thickness is 13 nm. Each sheet consists of 3 layers of Ti (red spheres) and 2 layers C (blue spheres). Either side of each flake has terminations T_x of OH, F and/or O, which react when plasma treated. At the corners of the rectangle the sample is clamped using Cu contacts, that are used for 4-point measurements of *IV*-curves in constant current mode.

2.1.3 Spincoating Ti_3C_2. Glass substrates were cut to $(2.5\ cm)^2$ in size and washed three times each with Hellmanex™ detergent, distilled water, and ethanol. Films were spin coated using approximately 0.3 ml of the solution at 800 rpm for 30 s then 2000 rpm for 5 s to remove any excess solution from the corners. Samples were covered in aluminium foil and stored in vacuum (10^5 Pa). For more details see the publication by Dillon *et al.*[26]

2.1.4 Thickness and transparency. The upper procedure gives transparent samples with a minor grey shade observed by eye. Their thicknesses were calculated from the absorbance spectra obtained from UV-VIS measurements, calibrated by atomic force microscopy (AFM) as described by Dillon *et al.*[26] The presented film had a transmittance of 65 ± 1%, which is correlated to an averaged thickness of 13 ± 1 nm by interpolating Fig. 5 in ref. 26. However, the roughness of the films may be larger than 1 nm. In plane dimensions were measured with a calliper (Fig. 1).

2.2 Measurements techniques

Schematics of the experimental setup are shown in Fig. 1 and 2. A vacuum chamber[43,44] with a base pressure of 5×10^{-7} Pa (5×10^{-9} mbar)¶ is pumped by a turbo pump‖ and a Titan sublimation pump. The latter is separated by a valve during plasma treatment and firing of the Titanium pump, to prevent Ti covering the sample.

To couple the electromagnetic waves to the gas in the vacuum chamber a metal glass adapter is surrounded by 6 windings of 5 mm copper tubes. A modified radio frequency (rf) generator** at 13.56 MHz is used to excite plasma in the glass

† Mesh hole diameter 44 μm, Sandvik™, Sweden.
‡ Alfa Aesar™, 99.5% purity.
§ Fisher™ TraceMetal grade.
¶ Measured by MKS™ PR 4000.
‖ Leybold™ Turbovac SL80.
** Hüttinger™ PFG 300 RF.

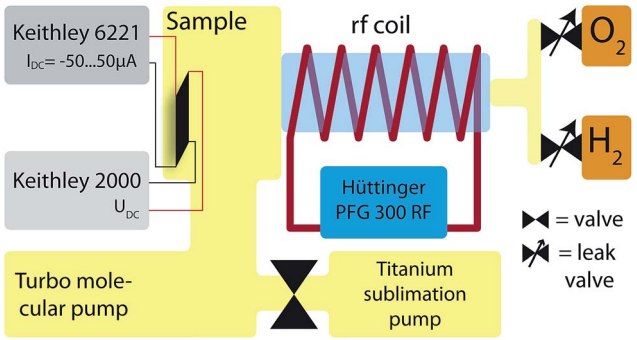

Fig. 2 Schematics of the setup. Yellow areas describe vacuum, light blue describes the glass tube with vacuum for exciting the plasma using the rf coil. This chamber is connected to a larger setup for investigating magnetic, chemical and structural properties.

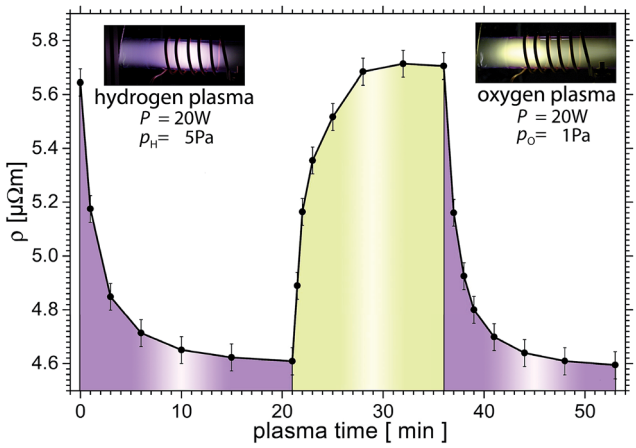

Fig. 3 Time dependence of resistivity as a function of plasma time. The H plasma decreases the resistivity, while the O one increases it. The as prepared resistivity value is slightly below the highest value shown here. Each data point results from fitting the slope of a bipolar *IV*-curve (±50 μA) of at least 10 data points. Using this resistance, Van-der-Pauw's method and the thickness of the sample, we evaluated the resistivity as plotted. When not measuring *IV* curves, the current was reduced to 2 μA. During measurement of the *IV*-curves, the rf-generator was switched off.

tube and chamber. Hydrogen (H) and oxygen (O) are connected to the chamber *via* two separate leak valves. At a pressure (p) of $p_H = 15$ Pa (0.15 mbar) for H and $p_O = 5$ Pa (5×10^{-2} mbar) for O of ≥99.998% purity, an rf power of 20 W was applied through the coil. When using the O plasma, the pressure was doubled for 1–3 seconds to get a more homogeneous plasma, especially at the samples position. At a distance of 30 mm from the sample a thermocouple was positioned to detect the temperature rise due to the plasma treatment. At 20 W and 40 W rf power (P) the temperature increases by 6 K and 10 K, respectively. 80% of the overall temperature change is reached after 10 min. It was shown, that using this setup nano structures can be reduced very well.[45]

The sample was 4-point-contacted at the corners of a rectangular film (see Fig. 1). Current (I)–voltage (V) curves were measured using a constant current (Keithley™ 6221) $I = -50\ldots50$ μA and a multimeter††. For more details see captions of Fig. 3 and 5.

XPS spectra were measured using non-monochromatic Al K_α radiation and a hemispherical electron energy analyzer.‡‡ Details are described in ref. 46. Here, is it better to say, that we used an *in situ* plasma treatment to judge the chemical changes and mimick the transport measurements. Ar sputtering is often used for cleaning, but our low energy plasma is more gentle, *i.e.* chemical etching instead of sputtering.

Humidity was measured by a commercial sensor§§ with a nominal detection range of 20–80$_{r.h.}$% and and error bar of 5%$_{r.h.}$.

3 Results

In Section 3.1 we describe the results of the plasma induced resistivity changes and in 3.2 we discuss results of the observed humidity induced changes. Both findings show the potential of using MXenes as materials for transparent gas and humidity sensors.

3.1 Plasma treated samples

3.1.1 Resistivity measurements. After more than 12 h in vacuum, the resistivity was measured in UHV after each H and O plasma treatment. In Fig. 3 we plot the resistivity as a function of time of plasma treatment. After one minute of H plasma, the resistivity was reduced by 8% from 5.64 μΩ m to 5.18 μΩ m. The error for each data point within the graph is <0.05 μΩ m (0.9%). Thus the relative change in resistivity of 8% is significant. The systematic error bar is estimated to 50% due to the unknown complex path of the currents through the MXene network.

Further H plasma treatment reduces the resistivity with an exponential decay down to 4.62 μΩ m. The resistivity decreases by 18% to 82% of the start value of 5.64 μΩ m within 11 min. We assume that in this step the known OH termination[23] reacts with H from the plasma to form steam, which is pumped away. H atoms may remain bonded at the MXene surfaces, however.

At $t = 21$ min in Fig. 3, the O plasma is switched on. Within one minute, the resistivity increases to 4.89 μΩ m. Further O plasma treatment increases the resistivity logarithmically as a function of time to 5.71 μΩ m which is similar to the initial value (only 1% above). Another series of H plasma treatments reduces the resistivity reproducibly to the previous H treated value to within <0.5%. Thus the resistivity of this MXene can be reversibly changed by 18%, presumably due to the removal of O that decreases the resistivity.

It is worth noting that when the same sample was treated with a power of 30 W an irreversible change, to higher resistivities values was observed presumably due to an irreversible oxidation of the MXene sheets.

3.1.2 X-Ray photoelectron spectroscopy. Reactive plasma etching is known to change the chemical state of samples

†† Keithley™ 2000 multimeter.
‡‡ SPECS™ XRC1000.
§§ Conrad Electronics™ HMZ-333A1.

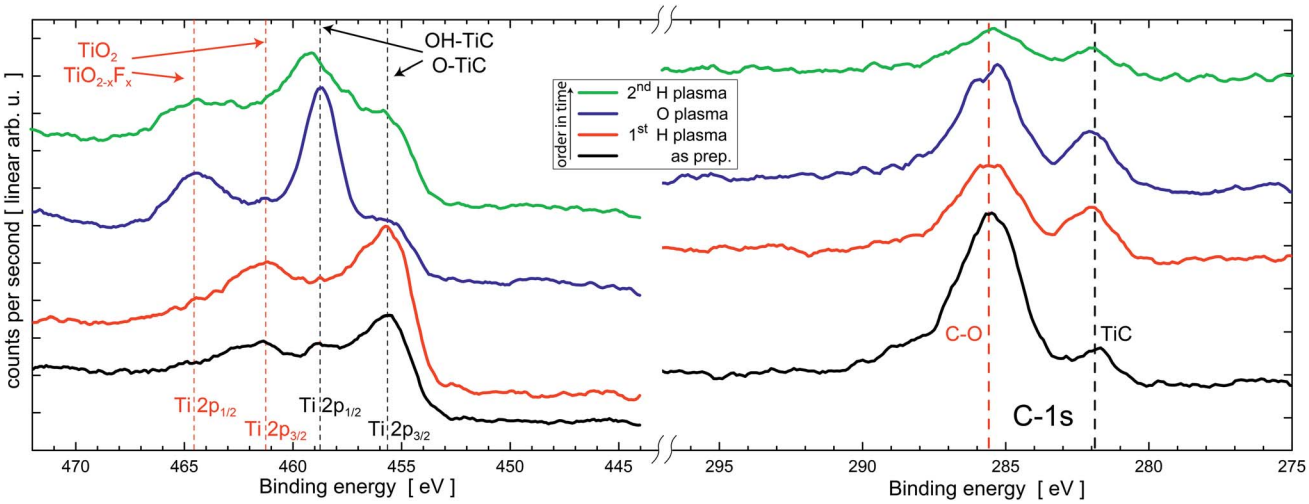

Fig. 4 XPS spectra of MXene after several plasma etching steps. Ti (2p peaks) and C (1s peak) indicate a gradual oxidation and removal of O after subsequent O and H plasma treatments at 20 W plasma power for 20 min, respectively. Vertical lines indicate reference values for various compounds from the literature[47] and ref. 23. After evaluation of the peak positions and intensities right (low binding energy) and left side (high binding energy) are individually scaled, shifted on the ordinate and smoothed using the Savitzky–Golay algorithm for better visualization. Quantitative analysis can be found in Table 1.

especially at the surfaces.[46] Here we track such changes by *in situ* plasma treatment and followed by XPS without breaking the vacuum of the Ti-2p and C-1s states in a different UHV system described by Wiedwald *et al.*[46] After the as prepared state is characterized, the plasma etching time is set to the final states in Fig. 3, *i.e.* after 20 min H plasma, after additional 20 min O plasma, and after a subsequent 20 min H plasma etching at a power of 20 W. The photoelectron spectra for the four states are shown in Fig. 4.

In the as prepared state, the XPS spectra of the Ti-2p region show peaks belonging to MXene (O, OH–Ti–C) and titanium oxide and oxyfluoride (TiO_2/$TiO_{2-x}F_x$),[23] while the C-1s has a prominent peak at about 286 eV belonging to C–O contamination and a smaller peak at 282 eV belonging to the carbide component in MXene as shown in Fig. 4. After the first H plasma treatment for surface cleaning and possible removal of O of the Ti_3C_2 films, we observe a reduction of the C–O component and a slightly increased intensity of the MXene peak at 282 eV. At 686 eV (not shown here) a small peak attributed to F is observed. This overall finding is ascribed to the removal of typical carbon containing surface contaminants after transfer in ambient conditions.

The peaks belonging to MXene are increased compared to those belonging to oxides and oxyflorides. Thus, H plasma etching does not change the chemical state of the Ti_3C_2 MXene significantly.

After O plasma etching the spectral weight of the TiO_2 and/or $TiO_{2-x}F_x$ component rises strongly while the residual TiC component decreases but remains clearly visible. The C-1s peaks remain more or less unchanged. The F peak vanishes in the noise. Subsequent H plasma does not completely reduce the specimen to its initial state, however, the spectral weight changes towards the Ti–C bonds providing possible evidence for a partial reversible removal of O.

The spectral weight of the different components (Ti–C and Ti–O_2) in the Ti-2p spectra are analyzed in more detail after subtracting the Shirley background for all sample states in Fig. 4. Within the error bar, and given quality of the data, the oxyfluoride content is not significant. It is therefore combined with TiO_2. Table 1 presents the results of this fitting. The error bar has been evaluated during fitting assuming certain spectral weights and direct comparison to the experiments.

As discussed above the relative weight of 69 ± 4% of TiC and 31 ± 4% TiO_2 components remains unchanged after H plasma treatment within the error bar. O plasma, however, oxidizes the Ti in the specimen significantly. The spectral weight of the oxide peaks increases to 67 ± 4%. Presumably the top and bottom layers of the Ti_3C_2 sheets are oxidized, thus changing the surface termination of MXenes. In turn, this observation explains the change in resistivity in Fig. 3. The underlying *I–V* curves suggest that subsequent H plasma treatment reduces the specimen to the initial state allowing for switching between high and low resistance states. XPS clearly shows this tendency. The initial state, however, is not reached after 20 min H plasma, and the result is a TiO_2 content of 54 ± 4%. These results are important because they suggest that it is possible to affect the transport properties of MXene films by changing their terminations. We note that at 3×10^{22} cm^{-3} the carrier densities in $Ti_3C_2T_x$ are quite high indeed and thus cannot be readily affected by changing the nature of the terminations.[26] The most likely mechanisms for the variations are

Table 1 Relative content of compounds determined from the intensities of different XPS peaks of Ti_3C_2 MXenes

State	TiC	TiO_2
As prep	69 ± 4%	31 ± 4%
After 1st H plasma	71 ± 4%	29 ± 4%
After 1st O plasma	33 ± 4%	67 ± 4%
After 2nd H plasma	46 ± 4%	54 ± 4%

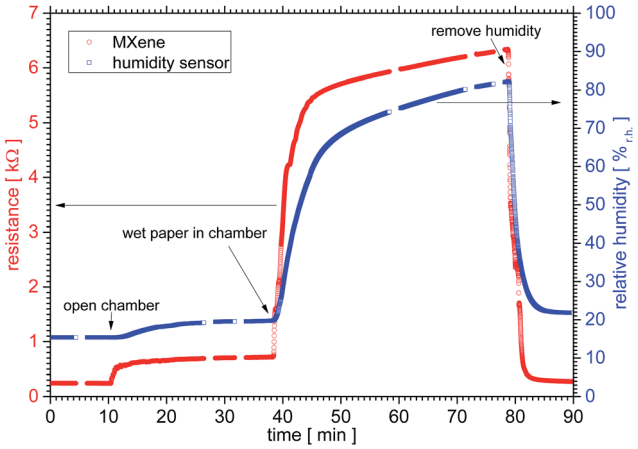

Fig. 5 Effect of the relative humidity on the resistance of a MXene film (red curve, left hand y-axis) and a humidity sensor (blue curve, right hand y-axis). Under a small N_2 flow the UHV chamber was opened at $t = 10$ min and the humidity increased slightly. At $t = 39$ min a wet towel was inserted in the chamber, which resulted in the humidity increases shown by the blue graph of the humidity sensor. At $t = 80$ min the paper was removed and the chamber was pumped down to a high vacuum. At all points a current of 2 μA was applied and the resistance was calculated by measuring V at this current only.

probably due to: (1) changing the resistance of the interlayer contacts (see below) and/or, (2) the electron mobilities are affected by plasma treatments.

3.2 Humidity dependent resistivity

When discussing MXene conductivity the surrounding humidity has to be taken into account, as Dillon *et al.*[26] have shown recently. The effect of humidity on the resistivity is shown in Fig. 5. The resistance changes when the environment is changed from dry nitrogen (N_2) to a relative humidity of 80 ± 5%$_{r.h.}$ by a factor of 26, namely from 243 Ω to 6341 Ω. The value is reversible – with a hysteresis smaller than the one of the commercial sensor described above.

For the analysis in Fig. 6 we chose data points at around $t =$ 9, 36, 50 and 75 min of Fig. 5, which represent constant values

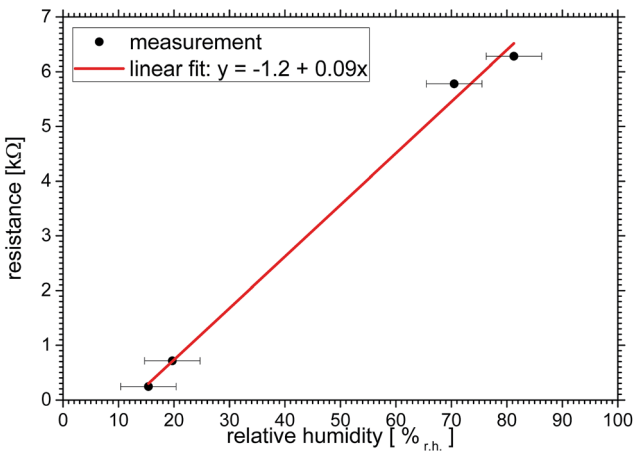

Fig. 6 Effect of relative humidity on MXene film resistance for some select data points taken from Fig. 5 at around $t = 9$, 36, 50 and 75 min.

of both curves. A linear fit of $y = -(1.2 \pm 0.3)$ kΩ + (0.094 ± 0.004) kΩ/%$_{r.h.}$ × x describes the resistivity *vs.* relative humidity reasonably well.

4 Discussion

We show that the plasma treatment results in a change of 18% in the resistivity by reducing or oxidizing the sample. At $P \leq 20$ W, the change is reversible, while at higher power the changes become, to some degree, irreversible. The XPS measurements show an irreversible behaviour, which does not reflect the observed resistivity changes. This is not too surprising since XPS only measures changes in the uppermost layers of the MXene film – that by its very nature is the most susceptible to oxidation – while the conductivity measurements reflect changes across the entire film.

The power dependence and the fact, that two different vacuum systems were used for the XPS and resistivity measurements, may explain this deviation since the plasma conditions may not have been identical. The XPS-chamber used a capacitive plasma, while the resistivity measurements were performed using an inductive plasma. The plasma excitation can be different at nominal identical powers and the vacuum system's geometry can also play a significant role.

Regarding the humidity sensor we would like to note that at nominally identical situations the MXene and commercial sensor show different values for two cases: in the beginning at $t = 0$ min under high vacuum condition the commercial sensor shows 15%$_{r.h.}$ and the MXene 0.243 kΩ respectively. At the end, again under high vacuum and after beeing exposed several times to a humid environment for $t = 90$ min, the values are 22%$_{r.h.}$ and 0.276 kΩ respectively. Although we did not measure it, we expect that after a long time both – commercial sensor and MXene film – would reach the original values $\rho(t = 0$ min). This is after 90 min not the case yet. Note that while the deviation from the initial conditions for the commercial sensor is 42%, the MXene's is only 13%. This suggests that at least under these conditions, the MXene film is a faster sensor.

That may be due to the fact that it is – compared to the MXenes – bulk like and moisture needs to diffuse through more material than in the 13 nm thick MXene film.

The linear behaviour of the MXene sensor has been shown within the error bar of 5%$_{r.h.}$ of the commercial sensor. Note that we expect flattening of the curves in Fig. 5 at low and especially high humidities. And while important this is beyond the scope of this paper. The origin of the changed resistivity due to humidity treatment could have the following reasons: the resistivity of the water itself influences the measurement, the macroscopic structure of the flakes is changed or the water reacts with the sample. Due to the MXene's relative chemical stability and the reversibility of the process we neglect the latter.

In the first case, water as a bad conductor may cover the sample. Using Kirchhoff's law, the resistivity should decrease or stay unchanged. The more likely effect, however, is that moisture is captured between the flakes reducing the interparticle contacts that in turn reduces the overall conductivity.

In summary we measured the changes in transport properties of thin spin-cast, 13 nm $Ti_3C_2T_x$ films as a function of plasma treatments and humidity. The results of this work are:

(1) It is possible to reversibly decrease the resistivity of our films by treating them with H-plasmas and increase it with O-plasmas. The changes with plasma treatment suggests a method to enhance the conductivity of these transparent, temperature stable and printable electrodes.

(2) By changing the humidity from that of dry N_2 to 80%$_{r.h.}$, the resistivity changed by a factor of 26. The response time of our films also appears to be somewhat faster than the commercial humidity sensor used herein. Our dynamic range – especially on the low humidity side – also appears to be strongly enhanced.

The ease by which these films can be made is an advantage over more sophisticated humidity sensors.[48] For example, the fact that our films can be readily printed renders them compatible with chip technology. Further, the direct change in resistivity may be useful for the low cost self-regulation of humidity in myriad applications. Before these applications can be realized, however, it is important to understand the long-term stability of these films, especially when continually exposed to humid air.

The $Ti_3C_2T_x$ films change their resistances when exposed to reactive H or O plasmas. They can thus, in principle, be used as H or O sensors. The resistivity of the MXene films was decreased by 18% by H plasma treatment in this very first experiment. In general it opens the route to increase the conductivity of these transparent, temperature stable and printable electrodes.

When taking both effects, humidity and reactives gases, into account, it is likely that the resistivity stems mainly from the overlapping areas of the flakes and not from the chemical structure itself. Therefore the irreversible chemical structure of the MXenes plays a subordinate role, but a reversible change in the termination appears to highly influence the conductivity. In other words, the resistivity seems to be controlled by the interfaces of the overlapping MXene flakes. To get a better insight into this we will investigate single flakes in the future.

5 Conclusion

For a 13 ± 1 nm thick spin-coated layer of two the dimensional Ti_3C_2 MXene flakes, we find a controllable change of 18 ± 1% in conductivity by selective O and H plasma treatment, rendering these structures interesting candidates for transparent H or O gas sensors. Secondly, a strong dependence of 2610 ± 10% on the relative humidity is observed which renders these transparent 2D flakes low cost and robust materials for miniaturized humidity sensors in, for example, food monitoring.

Acknowledgements

We would like to thank L. Schulte-Zweckel, Merve Alyazjie and Fangzhou Wang for assistance in the measurements.

References

1 M. Xu, T. Liang, M. Shi and H. Chen, *Chem. Rev.*, 2013, **113**, 3766–3798.
2 K. S. Novoselov, A. K. Geim, S. V. Morozov, D. Jiang, Y. Zhang, S. V. Dubonos, I. V. Grigorieva and A. A. Firsov, *Science*, 2004, **306**, 666–669.
3 Y. Liu, X. Dong and P. Chen, *Chem. Soc. Rev.*, 2012, **41**, 2283–2307.
4 X. Huang, Z. Zeng and H. Zhang, *Chem. Soc. Rev.*, 2013, **42**, 1934–1946.
5 Y. Shao, J. Wang, H. Wu, J. Liu, I. A. Aksay and Y. Lin, *Electroanalysis*, 2010, **22**, 1027–1036.
6 H. Xu, H. Dai and G. Chen, *Talanta*, 2010, **81**, 334–338.
7 Y. Wang, Y. Shao, D. W. Matson, J. Li and Y. Lin, *ACS Nano*, 2010, **4**, 1790–1798.
8 B. Su, J. Tang, J. Huang, H. Yang, B. Qiu, G. Chen and D. Tang, *Electroanalysis*, 2010, **22**, 2720–2728.
9 F. Schedin, A. K. Geim, S. V. Morozov, E. W. Hill, P. Blake, M. I. Katsnelson and K. S. Novoselov, *Nat. Mater.*, 2007, **6**, 652–655.
10 T. V. Cuong, V. H. Pham, J. S. Chung, E. W. Shin, D. H. Yoo, S. H. Hahn, J. S. Huh, G. H. Rue, E. J. Kim, S. H. Hur and P. A. Kohl, *Mater. Lett.*, 2010, **64**, 2479–2482.
11 W. Wu, Z. Liu, L. A. Jauregui, Q. Yu, R. Pillai, H. Cao, J. Bao, Y. P. Chen and S.-S. Pei, *Sens. Actuators, B*, 2010, **150**, 296–300.
12 G. Lu, K. Yu, L. E. Ocola and J. Chen, *Chem. Commun.*, 2011, **47**, 7761–7763.
13 M. Pumera and A. H. Loo, *TrAC, Trends Anal. Chem.*, 2014, **61**, 49–53.
14 Q. H. Wang, K. Kalantar-Zadeh, A. Kis, J. N. Coleman and M. S. Strano, *Nat. Nanotechnol.*, 2012, **7**, 699–712.
15 H. Li, Z. Yin, Q. He, H. Li, X. Huang, G. Lu, D. W. H. Fam, A. I. Y. Tok, Q. Zhang and H. Zhang, *Small*, 2012, **8**, 63–67.
16 Q. He, Z. Zeng, Z. Yin, H. Li, S. Wu, X. Huang and H. Zhang, *Small*, 2012, **8**, 2994–2999.
17 J. Feng, L. Peng, C. Wu, X. Sun, S. Hu, C. Lin, J. Dai, J. Yang and Y. Xie, *Adv. Mater.*, 2012, **24**, 1969–1974.
18 Z. Liu, S. P. Lau and F. Yan, *Chem. Soc. Rev.*, 2015, **44**, 5638–5679.
19 M. Naguib, V. N. Mochalin, M. W. Barsoum and Y. Gogotsi, *Adv. Mater.*, 2014, **26**, 992–1005.
20 M. W. Barsoum, *MAX Phases – Properties of Machinable Ternary*, Wiley-VCH, 2013.
21 M. Naguib, M. Kurtoglu, V. Presser, J. Lu, J. Niu, M. Heon, L. Hultman, Y. Gogotsi and M. W. Barsoum, *Adv. Mater.*, 2011, **23**, 4248–4253.
22 J. Halim, S. Kota, M. R. Lukatskaya, M. Naguib, M.-Q. Zhao, E. J. Moon, J. Pitock, J. Nanda, S. J. May, Y. Gogotsi and M. W. Barsoum, *Adv. Funct. Mater.*, 2016, **26**, 3118–3127.
23 J. Halim, K. M. Cook, M. Naguib, P. Eklund, Y. Gogotsi, J. Rosen and M. W. Barsoum, *Appl. Surf. Sci.*, 2016, **362**, 406–417.
24 J. Halim, M. R. Lukatskaya, K. M. Cook, J. Lu, C. R. Smith, L.-A. Näslund, S. J. May, L. Hultman, Y. Gogotsi, P. Eklund and M. W. Barsoum, *Chem. Mater.*, 2014, **26**, 2374–2381.
25 K. Hantanasirisakul, M.-Q. Zhao, P. Urbankowski, J. Halim, B. Anasori, S. Kota, C. E. Ren, M. W. Barsoum and Y. Gogotsi, *Adv. Electron. Mater.*, 2016, **2**, 1600050.

26 A. D. Dillon, M. J. Ghidiu, A. L. Krick, J. Griggs, S. J. May, Y. Gogotsi, M. W. Barsoum and A. T. Fafarman, *Adv. Funct. Mater.*, 2016, **26**, 4162–4168.
27 A. Ali, A. Belaidi, S. Ali, M. I. Helal and K. A. Mahmoud, *J. Mater. Sci.: Mater. Electron.*, 2016, **27**, 5440–5445.
28 Y. Xie, M. Naguib, V. N. Mochalin, M. W. Barsoum, Y. Gogotsi, X. Yu, K.-W. Nam, X.-Q. Yang, A. I. Kolesnikov and P. R. C. Kent, *J. Am. Chem. Soc.*, 2014, **136**, 6385–6394.
29 X. Liang, A. Garsuch and L. F. Nazar, *Angew. Chem., Int. Ed.*, 2015, **54**, 3907–3911.
30 D. Er, J. Li, M. Naguib, Y. Gogotsi and V. B. Shenoy, *ACS Appl. Mater. Interfaces*, 2014, **6**, 11173–11179.
31 M. R. Lukatskaya, O. Mashtalir, C. E. Ren, Y. Dall'Agnese, P. Rozier, P. L. Taberna, M. Naguib, P. Simon, M. W. Barsoum and Y. Gogotsi, *Science*, 2013, **341**, 1502–1505.
32 M. Ghidiu, M. Lukatskaya, M.-Q. Zhao, Y. Gogotsi and M. Barsoum, *Nature*, 2015, **516**, 78–81.
33 X. Xie, S. Chen, W. Ding, Y. Nie and Z. Wei, *Chem. Commun.*, 2013, **49**, 10112–10114.
34 O. Mashtalir, K. M. Cook, V. N. Mochalin, M. Crowe, M. W. Barsoum and Y. Gogotsi, *J. Mater. Chem. A*, 2014, **2**, 14334–14338.
35 Q. Peng, J. Guo, Q. Zhang, J. Xiang, B. Liu, A. Zhou, R. Liu and Y. Tian, *J. Am. Chem. Soc.*, 2014, **136**, 4113–4116.
36 A. Miranda, J. Halim, M. W. Barsoum and A. Lorke, *Appl. Phys. Lett.*, 2016, **108**, 033102.
37 F. Wang, C. Yang, C. Duan, D. Xiao, Y. Tang and J. Zhu, *J. Electrochem. Soc.*, 2015, **162**, B16–B21.
38 F. Wang, C. Yang, M. Duan, Y. Tang and J. Zhu, *Biosens. Bioelectron.*, 2015, **74**, 1022–1028.
39 B. Xu, M. Zhu, W. Zhang, X. Zhen, Z. Pei, Q. Xue, C. Zhi and P. Shi, *Adv. Mater.*, 2016, **28**, 3333–3339.
40 X.-F. Yu, Y. chun Li, J. bo Cheng, Z. bo Liu, Q. zhong Li, W. zuo Li, X. Yang and B. Xiao, *ACS Appl. Mater. Interfaces*, 2015, **7**, 13707–13713.
41 B. Xiao, Y. chun Li, X. fang Yu and J. bo Cheng, *Sens. Actuators, B*, 2016, **235**, 103–109.
42 M. Ghidiu, J. Halim, S. Kota, D. Bish, Y. Gogotsi and M. W. Barsoum, *Chem. Mater.*, 2016, **28**, 3507–3514.
43 F. M. Römer, Ph.D. thesis, Universität Duisburg-Essen, 2012.
44 F. M. Römer, M. Möller, K. Wagner, L. Gathmann, R. Narkowicz, H. Zähres, B. R. Salles, P. Torelli, R. Meckenstock, J. Lindner and M. Farle, *Appl. Phys. Lett.*, 2012, **100**, 092402.
45 C. Antoniak, M. E. Gruner, M. Spasova, A. V. Trunova, F. M. Römer, A. Warland, B. Krumme, K. Fauth, S. Sun, P. Entel, M. Farle and H. Wende, *Nat. Commun.*, 2011, **2**, 528.
46 U. Wiedwald, K. Fauth, M. Heßler, H.-G. Boyen, F. Weigl, M. Hilgendorff, M. Giersig, G. Schütz, P. Ziemann and M. Farle, *ChemPhysChem*, 2005, **6**, 2522–2526.
47 A. V. Naumkin, A. Kraut-Vass, S. W. Gaarenstroom and C. J. Powell, *NIST X-ray Photoelectron Spectroscopy Database V4.1*, 2012, http://srdata.nist.gov/xps/.
48 P. Faia, C. Furtado and A. Ferreira, *Sens. Actuators, B*, 2005, **107**, 353–359.